Smart Structures and Systems, *Vol. 24, No. 1 (2019) 95-110*
DOI: https://doi.org/10.12989/sss.2019.24.1.095

Studies on vibration control effects of a semi-active impact damper for seismically excited nonlinear building

Zheng Lu[*1,2], Hengrui Zhang[2] and Sami F. Masri[3]

[1]*State Key Laboratory of Disaster Reduction in Civil Engineering, Tongji University, Shanghai 200092, China*
[2]*Department of Disaster Mitigation for Structures, Tongji University, Shanghai 200092, China*
[3]*Sonny Astani Department of Civil and Environmental Engineering, University of Southern California, Los Angeles, CA 90089, USA*

(Received February 28, 2019, Revised March 8, 2019, Accepted March 10, 2019)

Abstract. The semi-active impact damper (SAID) is proposed to improve the damping efficiency of traditional passive impact dampers. In order to investigate its damping mechanism and vibration control effects on realistic engineering structures, a 20-story nonlinear benchmark building is used as the main structure. The studies on system parameters, including the mass ratio, damping ratio, rigid coefficient, and the intensity of excitation are carried out, and their effects both on linear and nonlinear indexes are evaluated. The damping mechanism is herein further investigated and some suggestions for the design in high-rise buildings are also proposed. To validate the superiority of SAID, an optimal passive particle impact damper (PID_{opt}) is also investigated as a control group, in which the parameters of the SAID remain the same, and the optimal parameters of the PID_{opt} are designed by differential evolution algorithm based on a reduced-order model. The numerical simulation shows that the SAID has better control effects than that of the optimized passive particle impact damper, not only for linear indexes (e.g., root mean square response), but also for nonlinear indexes (e.g., component energy consumption and hinge joint curvature).

Keywords: semi-active impact damper; particle damper; semi-active control, vibration mitigation; passive control, structural control

1. Introduction

Structures undergo vibrations in response to wind and earthquake excitations, which may lead to excessive lateral displacement or even collapse (Lu *et al.* 2016a). The debris of the collapsed structures has claimed many lives. Consequently, one of the main goals in structural engineering is to develop innovative vibration control devices (Housner *et al.* 1997, Spencer and Nagarajaiah 2003, Lu *et al.* 2017a, 2017f, 2018e, Xu *et al.* 2013, Nagarajaiah and Jung 2014a).

Tuned mass dampers (TMDs), a popular auxiliary-mass damping device, are passive control devices that have been applied extensively in practical high-rise buildings, such as the Shanghai Tower (Lu *et al.* 2017b) and the Taipei 101 building (Chung *et al.* 2013). Many experiments and simulations have been conducted to evaluate the performance of structures with a TMD system under various loads, and with various parameters (Bekdaş and Nigdeli 2013, Tributsch and Adam 2012, De Angelis *et al.* 2012), and many optimal formulas have also been proposed in the past decades (Tsai and Lin 1993, Fujino and Abe 1993, Bakre and Jangid 2007, Jonathan and Egidio 2016). When the frequency of vibrational TMD is tuned to the structural natural frequency, energy flows from the main structure to the TMD and then is dissipated by the damping unit, which is called the tuning effect. However, the effectiveness of a TMD depends on many factors, such as the characteristic of the excitation and the dynamic characteristic variation of the primary structure. Consequently, some improvements have been proposed to overcome the shortcomings of conventional TMDs, and the improvements mainly include passive control strategy, such as multiple tuned mass dampers (MTMD) (Bakre and Jangid 2004, Lu *et al.* 2017c), distributed tuned mass dampers (d-TMD) (Han and Li 2008), *et al.*, and semi-active control strategies (Sun and Nagarajaiah 2014a, Sun 2018, Lu *et al.* 2018a), such as the variable stiffness (Sun and Nagarajaiah 2014b), variable damping (Lin *et al.* 2010), adaptive length (Nagarajaiah and Pasala 2014b), phase control (Chung *et al.* 2013), *et al*.

Particle impact damping technology, another auxiliary-mass type passive control strategy, has been attracting more and more attention in recent years (Darabi and Rongong 2012, Egger and Caracoglia 2015, Nakamura and Watanabe 2016, Lu *et al.* 2016b, Fu *et al.* 2018). According to the number of the units within the container and the particles in each unit, the traditional particle impact dampers (PIDs) can be classified into four fundamental types: single-unit single-particle damper (impact damper), multi-unit single-particle damper, single-unit multi-particle damper (particle damper), and multi-unit multi-particle damper (Lu *et al.* 2018e), as shown in Fig. 1. Collisions of both, particles to particles and particles to the container, can provide damping effects, while collisions of particles to the container can provide both damping effects and nonlinear restoring forces (Lu *et al.* 2018d). With the advantages of simple configuration,

*Corresponding author, Professor
E-mail: luzheng111@tongji.edu.cn

ISSN: 1738-1584 (Print), 1738-1991 (Online)

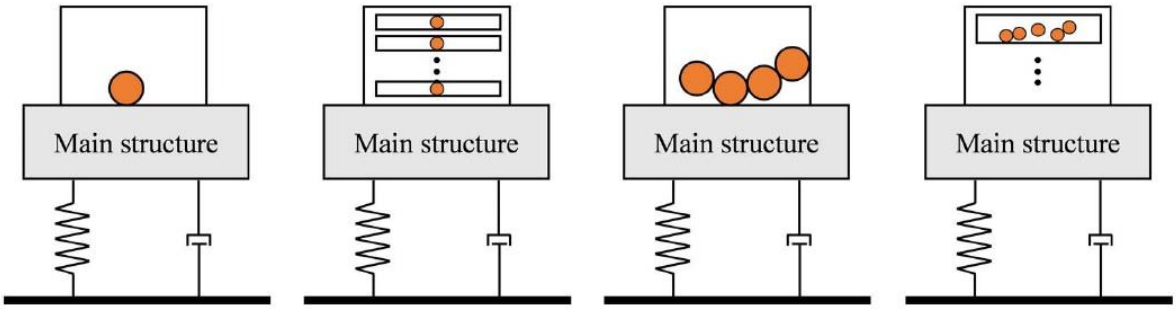

(a) single-unit single-particle damper (b) multi-unit single-particle damper (c) single-unit multi-particle damper (d) multi-unit multi-particle damper

Fig. 1 Schematic diagrams of traditional PIDs

considerable robustness, high reliability, maintenance-free operation, and wide-frequency band of vibration reduction (Lu *et al.* 2010, 2018b), it has been extensively applied in mechanical engineering and aerospace engineering (Ahmad *et al.* 2017, Wang *et al.* 2019). In recent years, many efforts have been invested in the application in the civil engineering field (Wang *et al.* 2016, Lu *et al.* 2017d, Zhang *et al.* 2018).

Owing to the discontinuous movement of the particles, vibration attenuation effects of traditional PIDs under relatively weak excitation conditions is not satisfactory, such as low frequencies and low amplitudes, especially in civil engineering. To solve this problem, some researchers proposed the use of particle tuned mass damper (PTMD) (Yao *et al. 2014*, Li and Tang 2017, Lu *et al.* 2017e), which combines both advantages of the particle damper and TMD, and the tuned liquid particle damper (TLPD) (Dai *et al.* 2017), which combines both advantages of particle damper and tuned liquid damper (TLD). In addition, collisions between particles and their container cannot always attenuate the response of the structure; the maximum efficiency of the particle damper can be achieved only when the excitation frequencies are near the resonant frequency of the main structure (Sanchez and Manuel Carlevaro 2013), which is familiar to the mechanism of TMD, termed as "tuning effect". Some researchers proposed a new concept of effective collisions (Cheng and Wang 2003, Lu *et al.* 2011, Afsharfard and Farshidianfar 2013), which is defined as the face-to-face collisions between the container and particles. Moreover, Masri *et al.* (1989) have shown that the maximum momentum transfer involved in the impact process can be achieved if the impacts occur at the instant of time corresponding to the peak velocity of the primary system, and proposed a semi-active control strategy for particle dampers (single-particle with single-unit or multi-unit) with adjustable motion-limiting stops (Masri *et al.* 1989, Masri and Chavakula 1994, Nayeri *et al.* 2007). Consequently, just like many scholars use semi-active control strategy to improve the performance of control devices (Xu *et al.* 2016a, 2016b), the semi-active impact damper (SAID) was preliminarily proposed here, and an impact is made to occur when the velocity of the main structure has reached its peak value.

Both simulations and experiments verified the effectiveness of the SAID, by linear single-degree-of-freedom (SDOF) primary structure and 3-story linear multi-degree-of-freedom (MDOF) primary structure. However, since the previous preliminary studies on SAID are restricted to a simple linear-elastic primary structure, the damping mechanism and vibration control effect on realistic nonlinear high-rise structures should be further investigated. Additionally, since practical engineering structures mostly undergo nonlinear behavior, because of both material nonlinearity and structural geometry nonlinearity under large seismic excitations, the effectiveness of such nonlinear behavior control in the main structure should also be taken into consideration.

Consequently, based on the previous studies, a configuration of semi-active impact damper compatible with a high-rise building is proposed, and the damping mechanism, as well as vibration control effects for a seismically excited nonlinear building, are investigated. The contents of this paper are arranged as follows: Section 2 presents the governing equations of the main structure with PID and SAID respectively, especially, the details of the semi-active strategy in the simulation is introduced. In Section 3, the effects of different parameters, including the mass ratio, damping ratio, rigid coefficient, and the intensity of the excitation, are investigated, both for linear and nonlinear indexes are compared here. To validate the superiority of SAID, Section 4 presents a comparable example between SAID and optimal PID, the optimal parameters of the PID are derived by a differential evolution (DE) algorithm based on a reduced-order model, and comparable parameters for the SAID are chosen, and both linear and nonlinear indexes at each floor are compared. In Section 5, some conclusions are presented.

2. Configuration model and semi-active control description

In this section, the system governing equation of a traditional particle impact damper (PID) is reviewed first, based on that, the difference between the PID and semi-

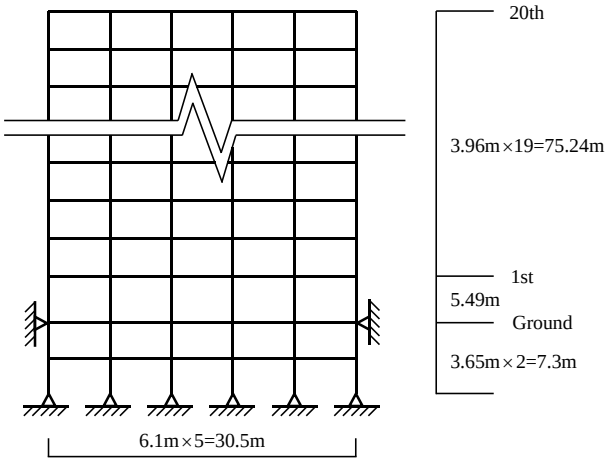

Fig. 2 Elevation of the N-S MRFs

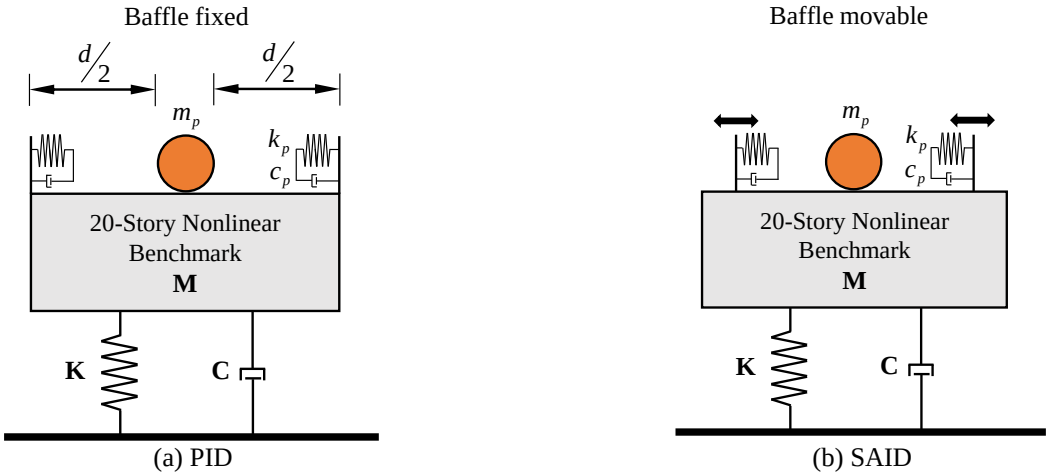

Fig. 3 Simplified diagram of the main structure with controller

active impact damper (SAID) is then discussed. Finally, the specific simulation details of SAID are set forth. Additionally, a detailed example comparison of the two control devices will be launched in Section 4.

In order to compare the vibration control effect of SAID, the 20-story nonlinear seismic benchmark building (Ohtori *et al.* 2004) that can resist the external horizontal loads, designed for the SAC Phase III Steel Project, is used in this paper. The benchmark building is 80.77 m in height, and its plane dimensions are 30.48 m × 36.58 m. The building has five bays each in the north-south (N-S) and six bays in the east-west (E-W) direction, and the bays are 6.10 m in all directions on the center. The lateral force-resisting system consists of steel perimeter moment-resisting steel frames (MRFs). The simulation study focuses on the in-plane analysis (N-S MRFs), and then the in-plane finite element model is analyzed. The elevation of the N-S MRFs is shown in Fig. 2. Taking the nonlinear response of the material into consideration, involves the moment-curvature bi-linear hysteresis model for structural components, and the concentrated plasticity model is utilized, whose plastic hinges only occur at the ends of the moment resisting beam-column and column-column joints and beams and columns are assumed to be elastic. The first ten natural frequencies of the 20-story nonlinear benchmark model are: 0.261, 0.753, 1.30, 1.83, 2.40, 2.44, 2.92, 3.01, 3.63 and 3.68 Hz, respectively. The numerical simulations are carried out by MATLAB and the SIMULINK platform. The simplified diagram of the main structure with PID and SAID are shown in Fig. 3, respectively. The system governing equation of PID can be written as Eqs. (1)-(4)

$$\begin{cases} \mathbf{M}\ddot{\mathbf{U}} + \mathbf{C}\dot{\mathbf{U}} + \mathbf{K}\mathbf{U} = \mathbf{M}\mathbf{E}\ddot{x}_g + \boldsymbol{\psi}F_p \\ m_p\ddot{u}_p + F_p = 0 \\ F_p = c_p H(y,\dot{y}) + k_p G(y) \end{cases} \tag{1}$$

$$\begin{cases} G(y) = \left[y - sgn(y) * \dfrac{d}{2} \right] * u(|y| - \dfrac{d}{2}) \\ H(y,\dot{y}) = \dot{y} * u(|y| - \dfrac{d}{2}) \end{cases} \tag{2}$$

$$\mathrm{sgn}(y) = \begin{cases} -1 & y < 0 \\ 0 & y = 0 \\ 1 & y > 0 \end{cases} \tag{3}$$

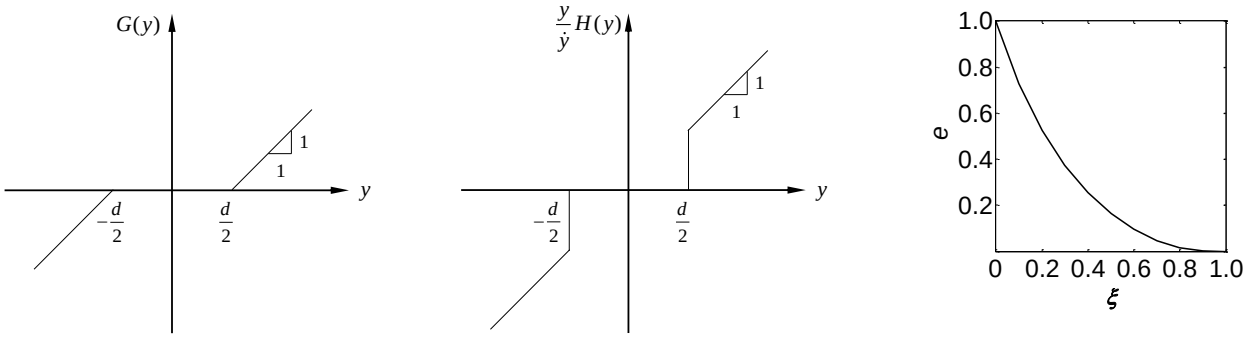

(a) stiffness function $G(y)$ (b) damping function $H(y,\dot{y})$ (c) relationship between the damping ratio ξ and the coefficient of restitution e

Fig. 4 Parameter relationship graph

$$\mathrm{u}(|y|-\frac{d}{2})=\begin{cases}1 & |y|-d/2>0\\ 0 & |y|-d/2\le 0\end{cases} \tag{4}$$

where $\mathbf{M},\mathbf{C},\mathbf{K}$ represent the mass, damping and stiffness matrices of main structure, respectively; $\mathbf{U},\dot{\mathbf{U}},\ddot{\mathbf{U}}$ are the displacement, velocity and acceleration vectors of main structure, respectively, $\mathbf{E}$ is the location vector of seismic force, $\boldsymbol{\psi}$ represents the location vector of the PID (For high-rise buildings, the first order mode usually contributes the most response, both PID and SAID are installed on the top layer in this investigation thus), $y=u_p-u_{top}$ represents the relative displacement of the particle with respect to the top floor, $G(y)$ and $H(y,\dot{y})$ are nonlinear functions in Eq. (2), as shown in Figs. 4(a) and 4(b), respectively. $[y-\mathrm{sgn}(y)*d/2]$ represents the overlapping distance in the collision process and $\mathrm{u}(|y|-d/2)$ is the collision indicator; d represents the gap clearance between the particle and the baffle, the gap clearance keeps in constant for the PID.

In addition, F_p represents the nonlinear restoring force between the main structure and the particle, including the nonlinear stiffness force and nonlinear damping force. k_p and c_p represent the stiffness and damping respectively, which can be used to simulate the interaction between the particle and the baffle: $k_p=m_p\omega_p^2$, $c_p=2\xi m_p\omega_p$ and $\omega_p=\lambda\omega_1$, where ω_1 represents the first-order frequency of the main structure. λ represents the rigid coefficient between the particle and the baffle, which can be used to simulate the baffle by a proper value; ξ represents the damping ratio, which can be used to simulate inelastic impacts, ranging from completely plastic to elastic impacts. In fact, the damping ratio is related to the well-known coefficient of restitution (Lu *et al.* 2017d), as shown in Fig. 4(c); thus, the value of any desired coefficient of restitution can be achieved by selecting the proper value for ξ.

The main difference of the SAID, compared to a conventional passive PID, is that the moment of an impact is adjustable. As mentioned above, an impact is made to occur when the velocity of the top floor of the main structure has reached its peak value, and the corresponding displacement of the top floor is equal to zero at the instant. Hence, the main governing equation of the SAID remains the same as PID (Eq. (1)) and the definition of gap clearance changes, which will be illustrated in the following simulation details.

The impacts will occur twice in a round-trip vibration, and the stability of this control strategy can be guaranteed, while the opposite condition of the relative velocity $\dot{y}$ and the absolute velocity $\dot{u}_{top}$ can be always satisfied. Diagrams of the impact process at the different moment are shown in Fig. 5, in which Figs. 5(a)-5(d) represents impact 1, Figs. 5(e)-5(h) represents impact 2. For instance, the whole process of impact 1 can be divided into four phases, just as shown in Figs. 5(a)-5(d), and the detailed information of simulation is discussed as follows:

(a) Start of the impact. The absolute displacement of the top floor is tracked, and we can determine an impact is happening when the absolute displacement cross zero, as shown in Fig. 5(a), the collision indicator can be expressed as Eq. (5)

$$v\left(u_{top}(t_n),u_{top}(t_{n+1})\right)=\begin{cases}1 & u_{top}(t_n)*u_{top}(t_{n+1})\le 0\\ 0 & u_{top}(t_n)*u_{top}(t_{n+1})>0\end{cases} \tag{5}$$

where $u_{top}(t_n)$ and $u_{top}(t_{n+1})$ represents the absolute displacements of the top floor at time t_n and t_{n+1}, respectively. The relative displacement $y(t_{n+1})$ between the particle and the top floor at time t_{n+1} is regarded as the new gap clearance in this impact.

(b) Overlapping and relative velocity $\dot{y}$ does not reverse, as shown in Fig. 5(b). At the time t_{n+i} $(i\ge 2)$, the overlapping distance can be expressed as

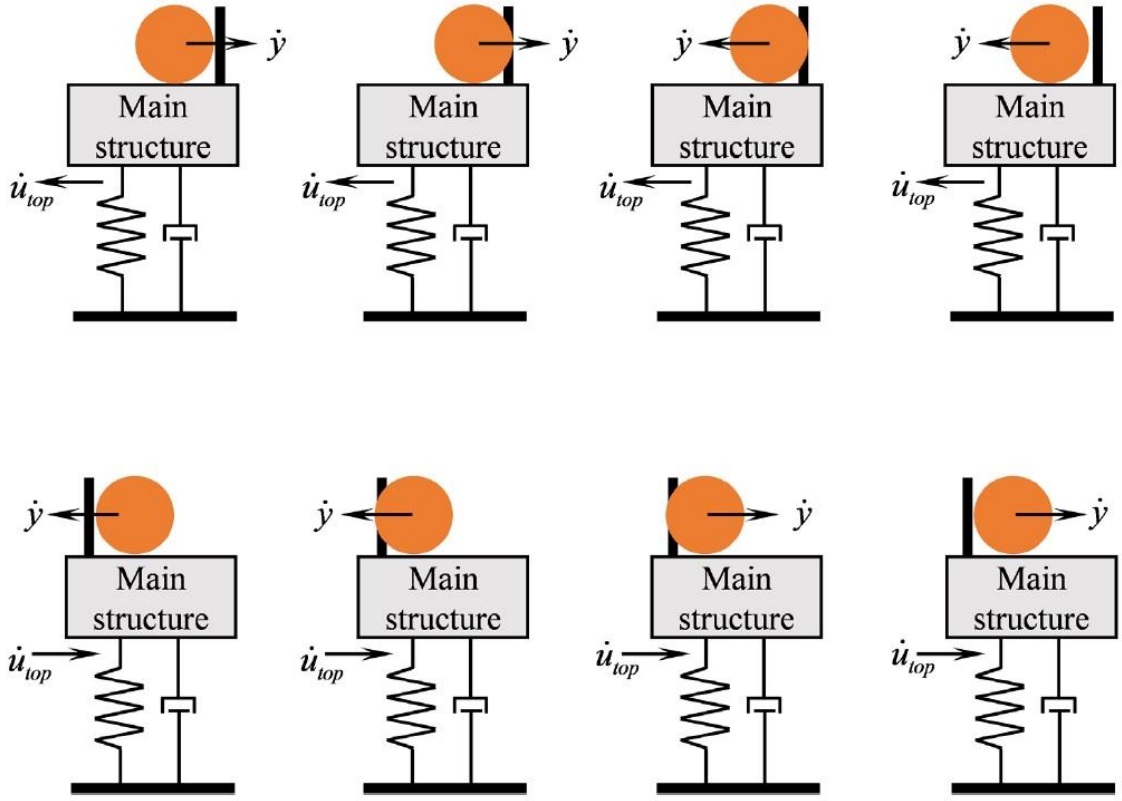

Fig. 5 Diagrams of the impact process at different moments: impact 1 (a)~(d); impact 2 (e)~(h)

$\left[y(t_{n+i})-y(t_{n+1})\right]$, which generates the nonlinear restoringforce. Nonlinear functions $G(y)$ and $H(y,\dot{y})$ in the whole impact process can be rewritten as follows

$$\begin{cases} G(y)=\left[y(t_{n+i})-y(t_{n+1})\right]^{*} v(u_{top}(t_n),u_{top}(t_{n+1})) \\ H(y,\dot{y})=\dot{y}*v(u_{top}(t_n),u_{top}(t_{n+1})) \end{cases} \quad (6)$$

Furthermore, the nonlinear stiffness force will increase and the nonlinear damping force will decrease in this process.

(c) Overlapping and relative velocity $\dot{y}$ reverses, as shown in Fig. 5(c). The nonlinear stiffness force will decrease with the decrease of overlapping distance according to Eqs. (1) and (6), and the nonlinear damping force reverses since the relative velocity $\dot{y}$ reverses.

(d) End of the impact, as shown in Fig. 5(d). The function $v\left(y(t_{n+i}),y(t_{n+1})\right)$ expressed in Eq. (7) is used to determine if the impact is over.

$$v\left(y(t_{n+i}),y(t_{n+1})\right)=\begin{cases} 1 & abs(y(t_{n+i}))\le abs(y(t_{n+1})) \\ 0 & abs(y(t_{n+i}))>abs(y(t_{n+1})) \end{cases} \quad (7)$$

In conclusion, combined with governing Eq. (1) and Eqs. (5)-(7), the response of the main structure with the SAID can be determined.

3. Parametric study for SAID

In this section, parametric studies are performed on the nonlinear benchmark building under discussion, with a semi-active impact damper (SAID), under El Centro wave with intensity 1.5 to enhance the understanding of the SAID behavior. According to the governing equations, some system parameters, such as mass ratio, the damping ratio of the particle, the rigid coefficient, can influence the nonlinear restoring force, and thus influence the seismic behavior of the nonlinear main structure. Therefore, these three parameters are investigated in this section. Additionally, some external parameters, such as excitation intensity are also investigated.

3.1 System parameters

The mass ratio μ is defined as the mass of the particle to the total mass of the main structure, for practical high-rise buildings, the mass ratio is usually less than 0.01, such as the Shanghai Tower. Thus, two mass ratios, 0.005 and 0.01, are chosen in this section for discussion. The rigid coefficient λ can be used to simulate the baffle with a proper value; similar to the coefficient of restitution, the damping ratio ξ can be used to simulate both elastic and inelastic impacts. For an impact damper, a larger nonlinear restoring force would cause a larger noise; hence the

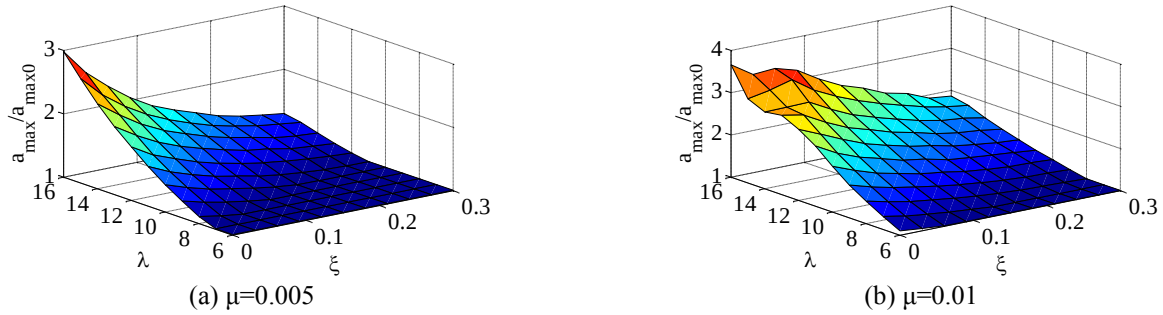

Fig. 6 Peak acceleration at the top floor with different mass ratio

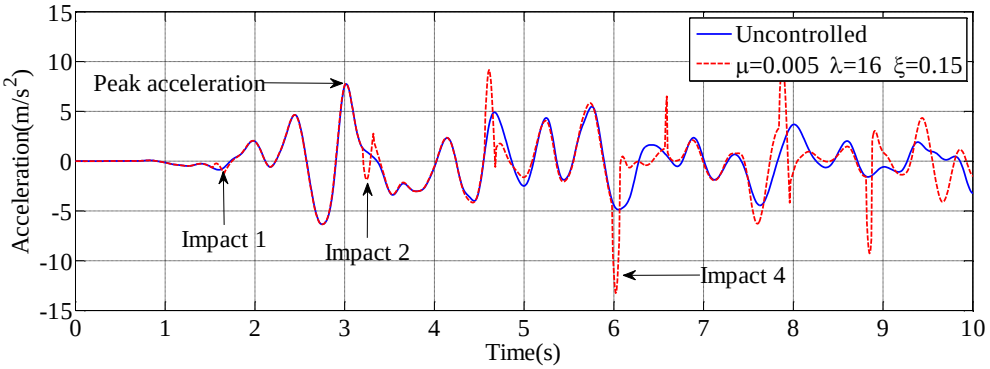

Fig. 7 Time-history response of acceleration at the top of the building

smaller rigid coefficient, ranges from 6 to 16 with the interval 1, is chosen, and the value of the damping ratio of the particle ranges from 0 to 0.3 with the interval 0.03, with totally 121 data points for each mass ratio.

To evaluate the vibration control effects of the SAID with different parameters, four linear indexes, including the peak acceleration (a_{max}), peak displacement (x_{max}), root-mean-square acceleration (RMS a) and root-mean-square displacement (RMS x), and three nonlinear indexes, including the number of plastic hinges (N_p), the total component energy consumption (N_e) and the maximum ratio of joint curvature (N_c), are investigated in this section. Note that the response of the top floor is the largest, which will affect the four linear indexes directly. Furthermore, all values (a_{max}, x_{max}, RMS a, RMS x, N_p, N_e, N_c) have been normalized by dividing by uncontrolled condition (a_{max0}, x_{max0}, RMS a_0, RMS x_0, N_{p0}, N_{e0}, N_{c0}).

3.1.1 Peak response

Fig. 6 shows the peak acceleration at the top floor. It can be seen that the control effect of SAID on peak acceleration is not good due to the sudden impact. To illustrate this phenomenon, time-history curves of acceleration at the top floor without control and with SAID (parameters: $\mu = 0.005,\ \lambda = 16,\ \xi = 0.15$) are shown in Fig. 7, and two factors have been summarized as follows:

(1) The peak acceleration of the main structure occurs at a very early time (around the 3rd second), and sufficient collisions between the particle and the baffle would take a few seconds. As shown in Fig. 7, only the inefficient impact 1 occurs before it, which has little influence on the time-history curve.

(2) When the nonlinear restoring force generated by the SAID with unsuitable parameters is too large, the peak acceleration can be amplified instead, such as the impact 4 in Fig. 7.

As the dark blue area is shown in Fig. 6, when the normalized value is close to 1, it indicates the factor (1) is the main factor; when the normalized value is larger than 1, it indicates the factor (2) is the main factor. In addition, the following rules can be summarized when the factor (2) is dominant:

(1) With a certain mass ratio μ, as the rigid coefficient λ increases, the peak acceleration increases; as the damping ratio ξ increases, the peak acceleration decreases; the influence of λ is more significant than ξ.

(2) With the increase of μ, the area originally dominated by the factor (1) has changed into factor (2), and the peak acceleration increases. In order to select parameters conveniently, a smaller μ is recommended.

The peak acceleration is proportional to the nonlinear restoring force at the top floor, which includes two parts: (a) nonlinear stiffness force F_{Ns}, and (b) nonlinear damping force F_{Nd}, which can be expressed as follows, respectively

$$F_{Ns} = k_p G(y) = m_p \omega_p^2 G(y) = m_p \omega_1^2 \lambda^2 G(y) \tag{8}$$

$$F_{Nd} = c_p H(y, \dot{y}) = 2\xi m_p \omega_p H(y) = 2m_p \omega_1 \lambda \xi H(y, \dot{y}) \tag{9}$$

The influence of parameter variation on the nonlinear restoring force is mainly reflected in two aspects: (1) Direct influence, such as λ and ξ; (2) Indirect influence, such

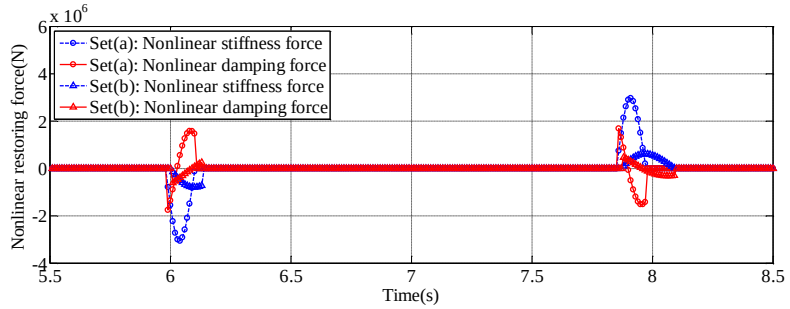

(a) λ

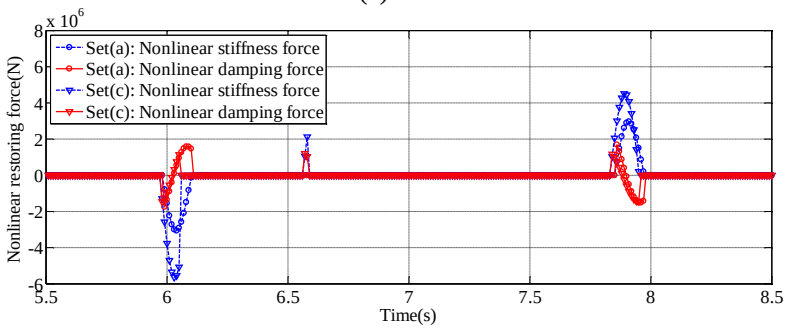

(b) ξ

Fig. 8 Nonlinear stiffness force and nonlinear damping force with different parameters

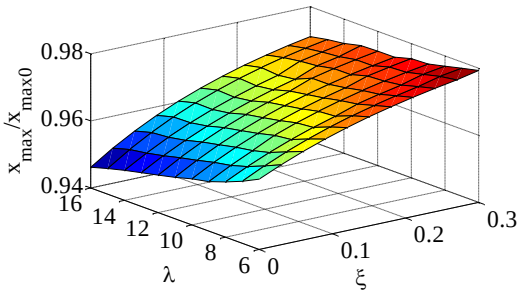

(a) μ=0.005

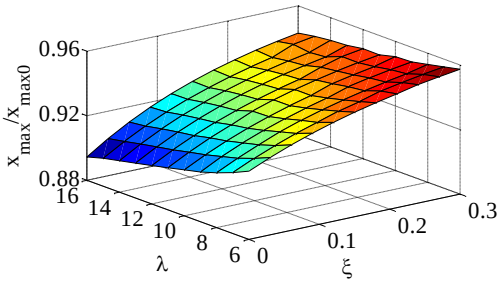

(b) μ=0.01

Fig. 9 Peak displacement at the top floor with different mass ratio

as the nonlinear function $G(y)$ and $H(y,\dot{y})$. In order to unify these two aspects into the effect of parameter variation, three sets of parameters are investigated: (a) $\mu=0.005,\ \xi=0.3,\ \lambda=16$; (b) $\mu=0.005,\ \xi=0.3,\ \lambda=8$; (c) $\mu=0.005,\ \xi=0.15,\ \lambda=16$. Set (a) and set (b) can be utilized to investigate the influence of λ, while set (a) and set (c) can be utilized to investigate the influence of ξ. Fig. 8 shows nonlinear stiffness force and nonlinear damping force with different parameters. It can be summarized that:

(1) As the increase of λ, both nonlinear forces show quadratic growth;

(2) As the decrease of ξ, nonlinear stiffness force shows proportional growth, while the nonlinear damping force declines slowly.

Fig. 9 shows the peak displacement at the top floor. It can be seen that no adverse effect on peak displacement is observed. This is because the relative velocity between the particle and the baffle $\dot{y}$ is always opposites to the absolute velocity $\dot{u}_{top}$ at the top floor, and the nonlinear restoring force attenuates the vibration with no doubt. Similarly, some rules can be summarized as follows:

(1) The SAID has a certain control effect on peak displacement.

(2) With a certain μ, as λ increases, the peak displacement decreases; as ξ increases, the peak displacement increases; the influence of λ is more significant than ξ.

(3) From the comparison of the ordinates of Figs. 9(a) 9(b): as the increase of mass ratio, the peak displacement decreases.

In combination with the previous discussion of peak acceleration, these rules actually indicate the fact that larger nonlinear restoring force will have a better control effect on the reduction of peak displacement.

3.1.2 RMS response

Due to the damping mechanism and physical nature of

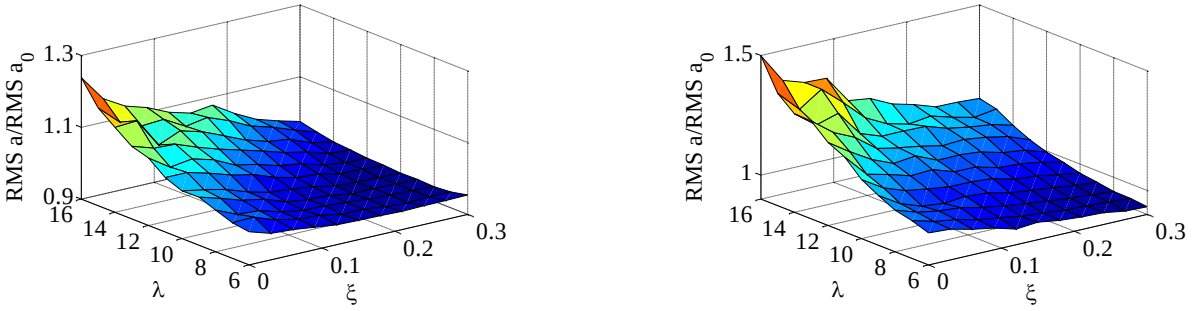

(a) μ=0.005 (b) μ=0.01

Fig. 10 RMS acceleration at the top floor with different mass ratio

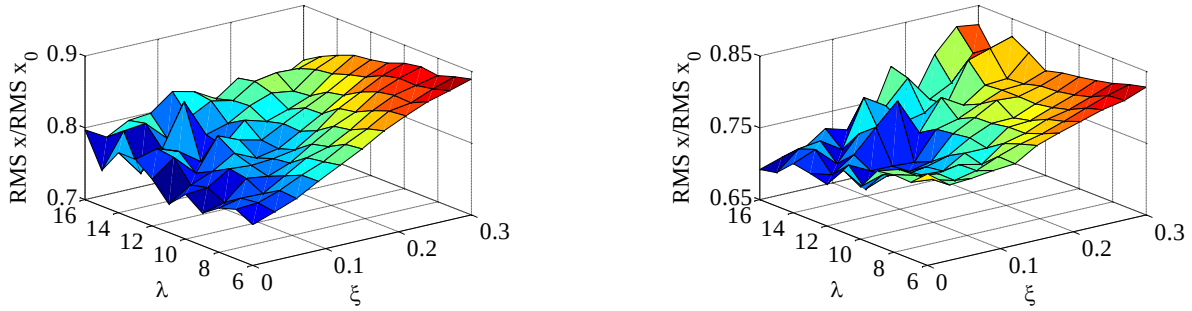

(a) μ=0.005 (b) μ=0.01

Fig. 11 RMS displacement at the top floor with different mass ratio

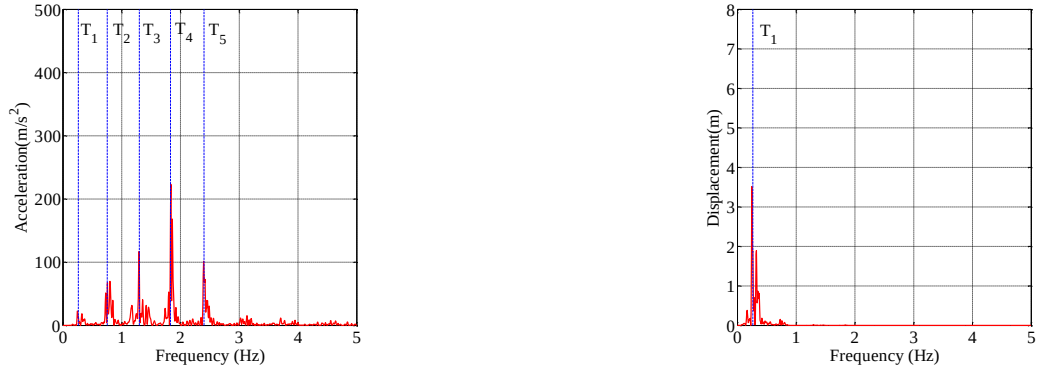

(a) acceleration (b) displacement

Fig. 12 Fourier spectrums of the time-history curve at the top floor $\left(set(c):\ \mu=0.005,\ \xi=0.15,\ \lambda=16\right)$

the device performance, the basic rules of RMS response remain generally the same as peak response. The RMS responses are shown in Fig. 10 and Fig. 11. However, some interesting phenomena in comparison to the peak response are pointed out as follows:

(1) As shown in Fig. 11, the associated surfaces are not as smooth as those for the peak response; this is because the peak response is the only response at a moment, while the RMS response has the relationship with all time-history response. Some impacts would have a little adverse effect on the RMS response, such as fluctuating at zero, but it does not affect the general trend.

(2) Compared with the peak acceleration, it has a certain control effect on the RMS acceleration, but the control effect is still not good, while the control effect on the RMS displacement is satisfactory. For instance, the normalized value in Fig. 11(b) is close to 0.7 with mass ratio 0.01, which means the RMS response can be reduced by 30%.

(3) Moreover, the Fourier spectrums of the time-history curve on the top floor are shown in Fig. 12; it indicates that the acceleration is controlled by higher-order modes, while the displacement is controlled by the first-order mode (Wongprasert and Symans 2004). Since the SAID is installed on the top floor, the control effect on acceleration

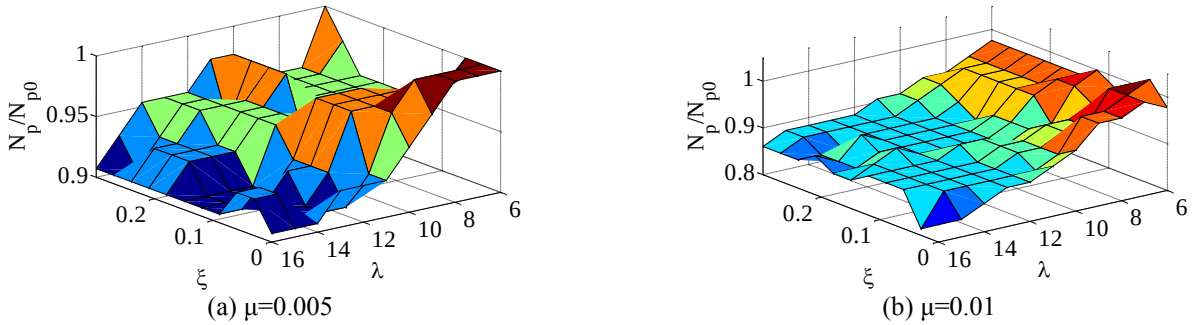

Fig. 13 Number of plastic hinges of the main structure with different mass ratio

hinges, total component energy consumption, and the

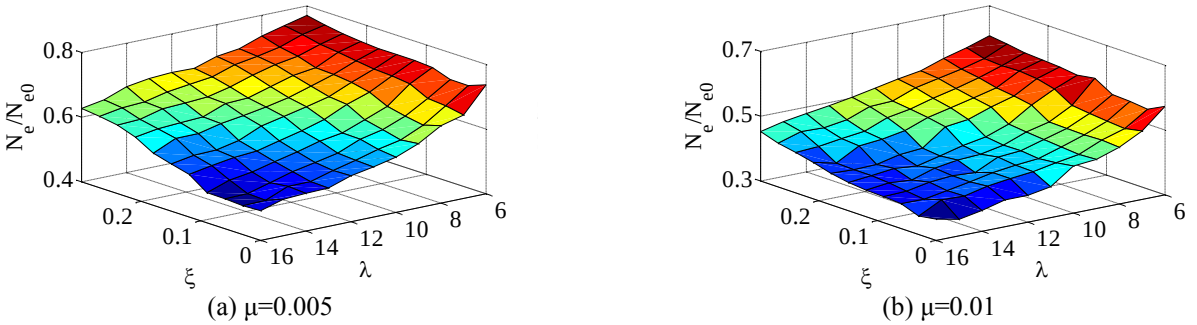

Fig. 14 Total component energy consumption of the main structure with different mass ratio

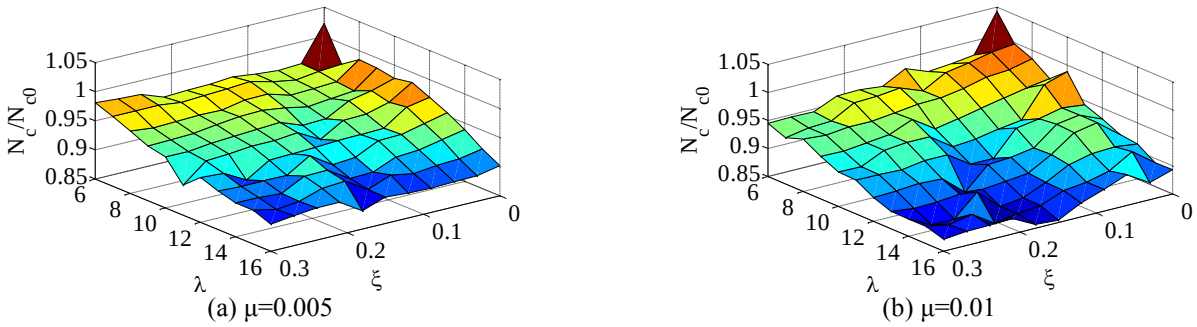

Fig. 15 Maximum ratio of joint curvature of the main structure with different mass ratio

is not good thus. If the damper is installed at the place corresponding to the fourth-order mode (10th and 16th floor), the acceleration control effect would be much better.

3.1.3 Nonlinear indexes

Three nonlinear indexes, including the number of plastic maximum ratio of joint curvature, are investigated here. The simulation results are shown in Figs. 13-15. Some conclusions can be summarized as follows:

(1) As the mass ratio μ increases, the control effects improve, including less number of plastic hinges, lower total component energy consumption and a smaller maximum ratio of joint curvature. However, the rate of improvement of the control effect is significantly lower than the increase rate of μ.

(2) The number of plastic hinges and the maximum ratio of joint curvature are not sensitive to the damping ratio ξ, and mainly influenced by the rigid coefficient λ. As the λ increases, the number of plastic hinges and the maximum ratio of joint curvature decrease.

(3) Total component energy consumption is one of the most important nonlinear indexes, and it shows the same rules as linear indexes: as the λ increases and ξ decreases, this index decreases.

The contour lines of both the momentum exchange between the particle and the main structure and the total component energy consumption (shown in Fig. 14) of the main structure are shown in Figs. 16 and 17, respectively. The general trend of the total component energy consumption is opposite to the momentum exchange, which

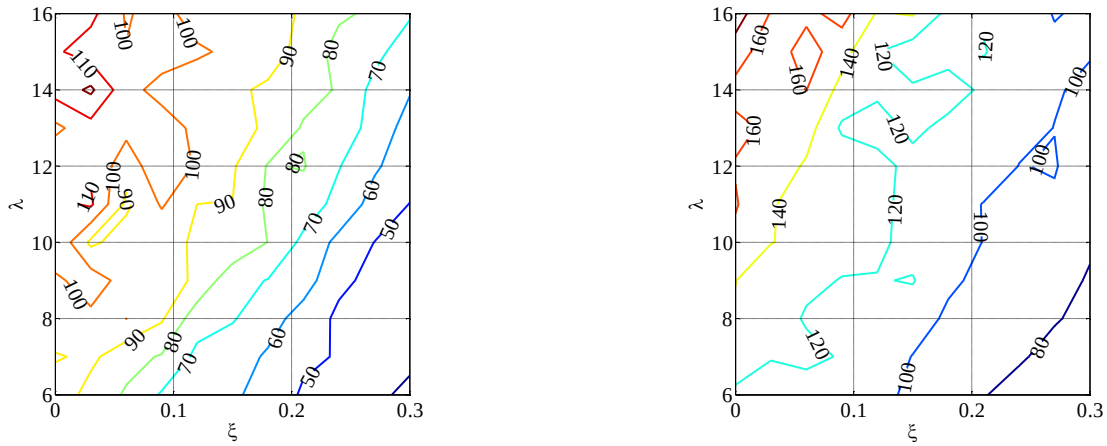

(a) μ=0.005 (b) μ=0.01

Fig. 16 Contour line of momentum exchange $(\times 10^5 kg gm/s)$ between the particle and the main structure with different mass ratio

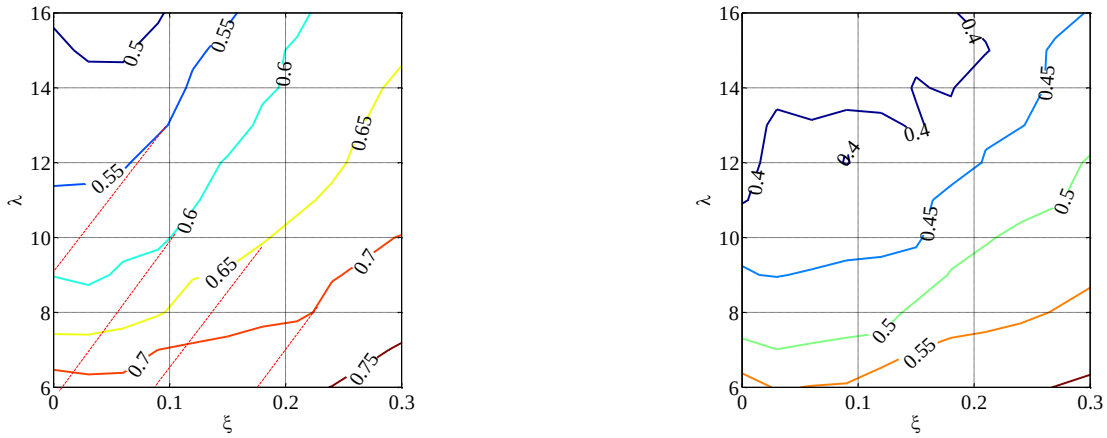

(a) μ=0.005 (b) μ=0.01

Fig. 17 Contour line of total component energy consumption of the main structure with different mass ratio

means effective momentum exchange can reduce the damage to the main structure, leading to a better vibration control effect. Moreover, the shape of the contour line in Fig. 16 is close to a straight line, while the shape of the contour line in Fig. 17 ($\xi < 0.2$) has a bit difference in lower damping ratio area. For instance, the points on the dashed line have similar momentum exchanges, as shown in Fig. 17, but the control effect on the total component energy consumption decreases with the decreasing of damping ratio, which indicates the damping ratio also plays an important role in the energy dissipation.

3.2 Excitation intensity

The analysis of the system parameters is based on the El Centro wave with intensity 1.5; thus, it is necessary to study the influence of the excitation intensity on the vibration control effect. Therefore, intensity levels of 0.5, 1.0 and 1.5 are considered in this section, and three basic methods can be used to investigate the effect of intensity:

(1) Keeping ξ and λ as constants 0.1 and 10, respectively, and changing μ;

(2) Keeping μ and λ as constants 0.01 and 10, respectively, and changing ξ;

(3) Keeping μ and ξ as constants 0.01 and 0.1, respectively, and changing λ;

All values have been normalized by dividing by the corresponding uncontrolled condition. For instance, the results of the RMS displacement are shown in Fig. 18. The curves of intensity 0.5 and intensity 1.0 are completely overlapping, which indicates the control effects of SAID is very stable in the elastic stage. While the main structure undergoes the nonlinear stage, the trend is consistent with the elastic stage. To summarize, the SAID is not sensitive to the increase of the excitation intensity, and certain control index even improves, such as the RMS x. Additionally, Fig. 18(a) is also a supplement proof for the mass ratio in section 3.1. When the mass ratio is greater than 0.01, the growth rate of the control effect on the RMS displacement is obviously lower than the growth rate of the mass ratio.

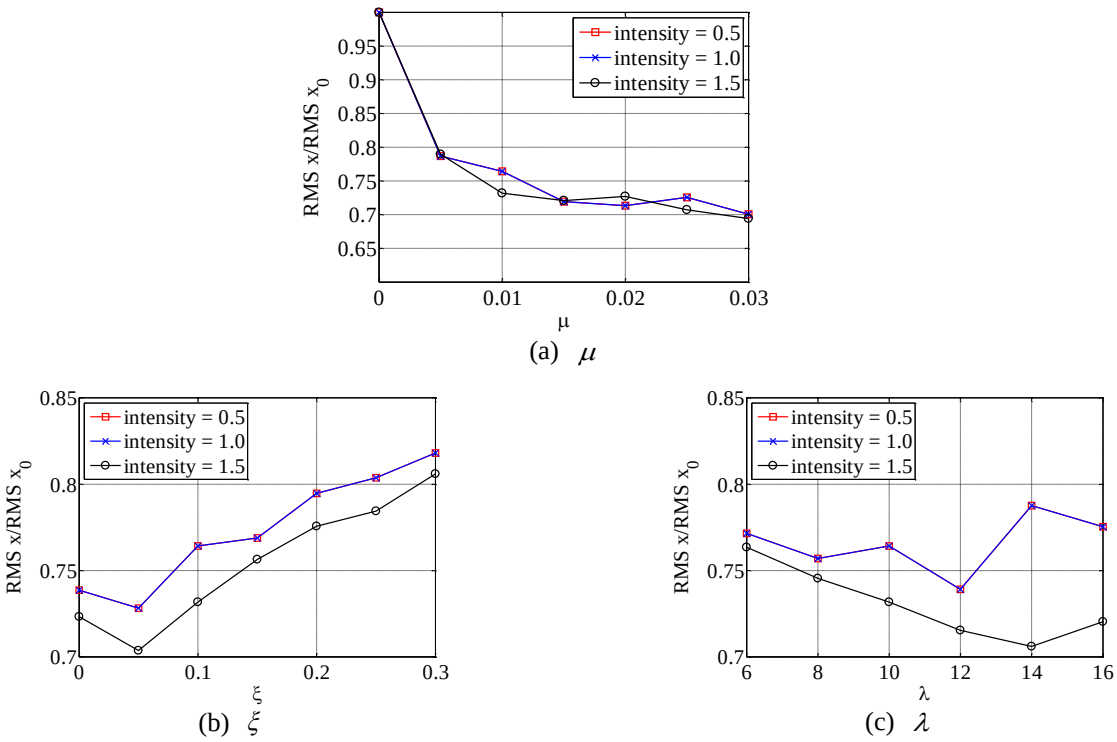

(a) μ (b) ξ (c) λ

Fig. 18 Intensity influence on RMS displacement with variable parameters

3.3 Discussion

Based on the extensive parametric study on SAID, some damping mechanism rules indicating its physical performance can be summarized as follows:

(1) As the mass ratio increases, the control effects on displacement response and all nonlinear indexes improve, however, the efficiency of improvement is obviously lower than the increase rate of mass ratio when the mass ratio is larger than 0.01.

(2) As the damping ratio increases, the control effect on the acceleration response is better, while the control effectson the displacement and total component energy consumption are worse, and the control effects on the number of plastic hinges and the maximum ratio of joint curvature change little. Moreover, increasing the damping ratio is beneficial to energy consumption when the damping ratio is lower than 0.2.

(3) As the rigid coefficient increases, the control effect on displacement response increases as well as the nonlinear behavior of the main structure improves. This parameter is more sensitive than the damping ratio.

(4) The influence of these parameters is actually the influence on the nonlinear restoring force, which reflecting the control mechanism for the damper.

(5) The intensity of excitation has generally no influence on the control effect under the elastic phase.

Taking this nonlinear structure as an example, some suggestions for practical design steps are proposed:

(1) Choose an appropriate mass ratio. It not only determines the range of parameters selection, but also controls the cost. Therefore, regarding no adverse effects on the acceleration control as a goal, the mass ratio can be chosen in advance, and also leaving enough range for other parameters. For illustration, the mass ratio is ideally less than 0.01 in this paper.

(2) For a better dissipation effect on the energy derived from momentum exchange, a suitable damping ratio is selected. For instance, the damping ratio should be larger than 0.2 in this investigation.

(3) Calculate the maximum inertia force at the top floor with a certain intensity, then the value of the rigid coefficient can be determined by meeting the condition that the nonlinear restoring force equals to the maximum inertia force.

4. Comparison between the SAID and PID_{opt}

To further understand the damping performance and also validate the superiority of the SAID, the optimal parameters of the passive impact damper (PID) are determined, while the parameters of the SAID remain the same. To evaluate the vibration control effects of the SAID, two linear indexes, including the root-mean-square (RMS) acceleration and RMS displacement along the height, and three nonlinear indexes, including the number of plastic hinges, component energy consumption of the main structure and the maximum ratio of joint curvature, are investigated. In addition, the El Centro wave with intensity 1.5 is utilized in this section.

4.1 Optimization methods

Since the original finite element (FE) model of this 20-story nonlinear building has a large number of degrees of freedom, the optimization of the particle impact damper

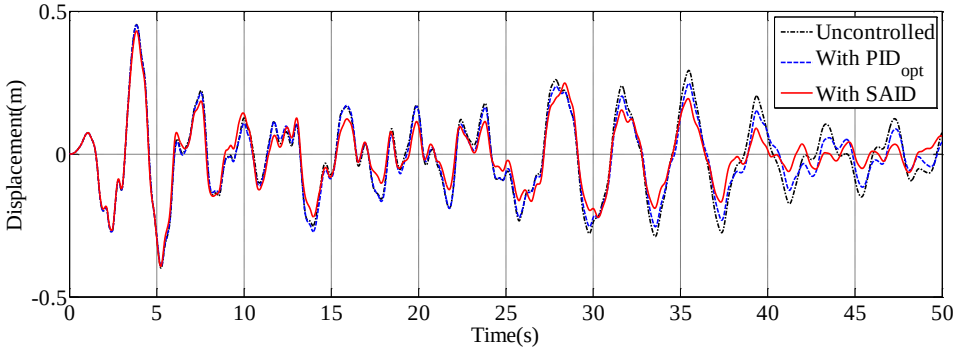

Fig. 19 Comparison of the displacement response at the top of the building under El Centro wave

Table 1 Parameters of PID and SAID

Controllers	λ	μ	ξ	d (m)
PID	6	0.01	0.2316	0.8192
SAID	6	0.01	0.2316	—

(PID) will cost a lot of time; thus, a reduced-order model is used here, based on differential evolution (DE) algorithm. More details about the parameter identification for thereduced-order and DE algorithm can be found in the reference (Lu *et al.* 2018c). The optimal parameters of PID are also determined by DE algorithm, and the optimal parameters of PID include the rigid coefficient, gap clearance, mass ratio and damping ratio of the particle. Considering that the RMS displacement response at the top floor is very important for the structural design, the detailed optimization process of PID is as follows

$$\min\ J(z) = abs[J_1(z) - J_{obj}] \tag{10}$$

$$J_1(z) = \frac{abs[RMS(u_{top}(t)) - RMS(u_{top}(z,t))]}{RMS(u_{top}(t))} \tag{11}$$

$$z = (\mu, \lambda, \xi, d) \tag{12}$$

where $J_{obj} = 0.6$ represents objective vibration control effect of the PID; $J_1(z)$ represents vibration control effect of the PID; $u_{top}(t)$ represents displacement response at the top of the main structure without control; $u_{top}(z,t)$ represents displacement response at the top of the main structure with the PID; z represents parameters vector of the PID. According to Section 3, the mass ratio is preset to 0.01. Table 1 shows the optimal parameters of PID while the parameters of SAID is determined the same as PID's. These parameters are also rational for SAID according to the discussion in Section 3.3.

4.2 Control effects comparison

To compare the performance of optimal PID (PID_{opt}) and SAID, the vibration control effect and the improvement rate are first defined as Eqs. (13) and (14)

$$\text{Vibration control effect (VCE)} = \frac{\text{the RMS of structure without control - the RMS of structure with PID/SAID}}{\text{the RMS of structure without control}} \tag{13}$$

$$\text{Improvement rate} = \frac{\text{the VCE of the structure with PID - the VCE of the structure with SAID}}{\text{the VCE of the structure with PID}} \tag{14}$$

The time-history curve of the displacement under El Centro wave at the top of the building is shown in Fig. 19, and three operating conditions (uncontrolled case, with PID_{opt} case and with SAID case) are compared. At the beginning of the excitation, the control effects of both PID_{opt} and SAID can be ignored, owing to the fact that sufficient impacts between the particle and the baffle would take a few seconds. As time progresses, the control effect is getting better.

The RMS response of each floor of the main structure subjected to El Centro wave are shown in Fig. 20. It can be seen that both the PID_{opt} and SAID can reduce the response along the structural height, in which the SAID performs better. From Fig. 20(a), it can be seen that the maximum vibration control effect on RMS acceleration for PID and SAID is 3.5% and 12.8% occurred at floor 19 and 7, respectively, and the improvement rate of the SAID compared with the PID_{opt} can reach 366%. The maximum vibration control effect on RMS displacement response at floor 20 for PID_{opt} and SAID can reach 7.5% and 19.2%, respectively, and the improvement rate of the SAID compared with the PID_{opt} can reach 256%, which validates the superiority of the SAID.

Fig. 21 shows the inter-story drift ratio of each floor of the main structure subjected to El Centro wave. It can be seen that compared to PID_{opt} case and uncontrolled case, the SAID case can largely reduce the inter-story drift ratio for many stories.

Considering material nonlinear state and the damage mechanism of beam hinge, some nonlinear performance indexes are investigated, including the number of plastic hinges, component energy consumption, and the maximum ratio of joint curvature. The number of plastic hinges and component energy consumption of each floor of the main structure under El Centro wave is shown in Fig. 22. It can

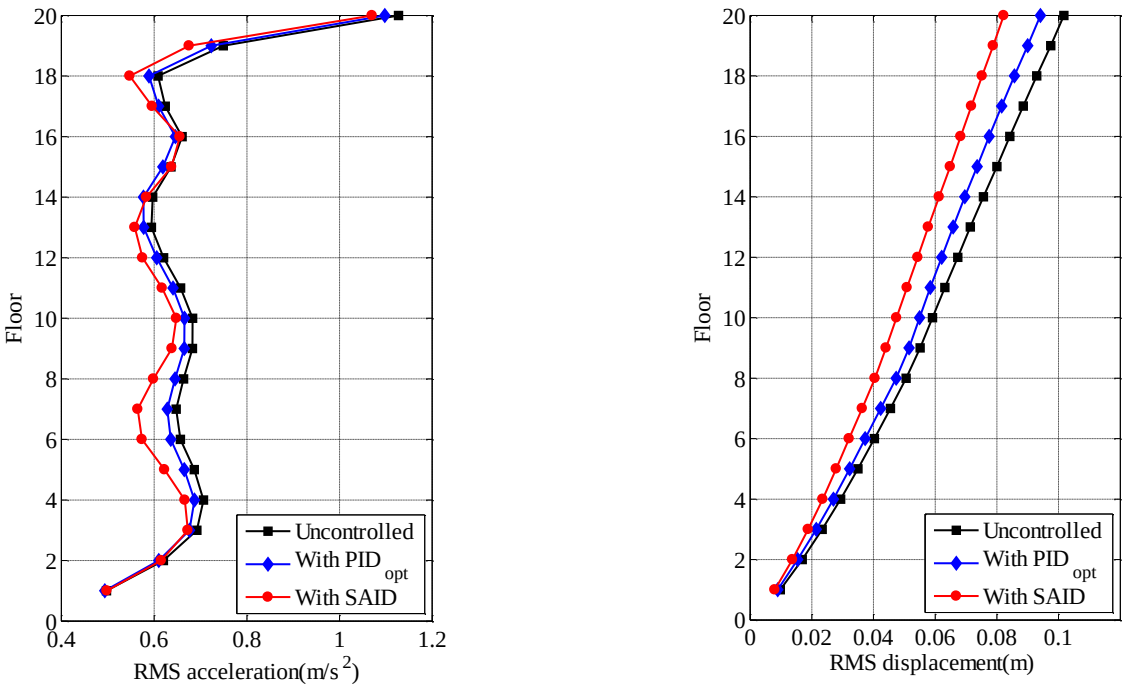

(a) acceleration (b) displacement

Fig. 20 RMS response of the main structure under El Centro wave

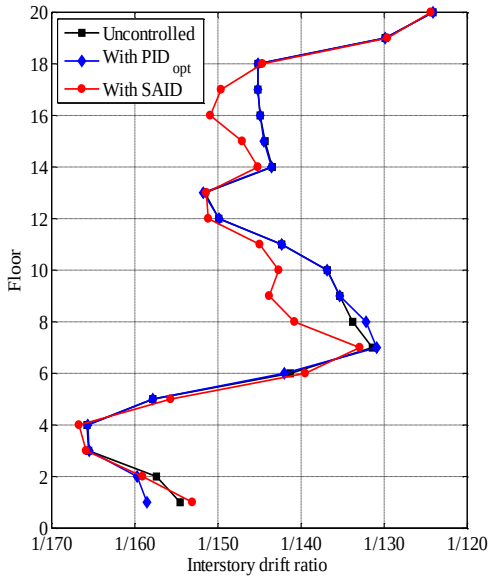

Fig. 21 Comparison of the inter-story drift ratio under El Centro wave

be seen that, although the number of plastic hinge for SAID case is equal to PID_{opt} case, the component energy consumption is largely reduced, indicating that the input energy flows to SAID greatly, hence protecting the main structure.

Fig. 23 shows the maximum ratio of joint curvature under El Centro wave. The results are consistent with that of component energy consumption, the structural damage under SAID case is much smaller than the PID_{opt} case, hence is much easier to be repaired after the earthquake.

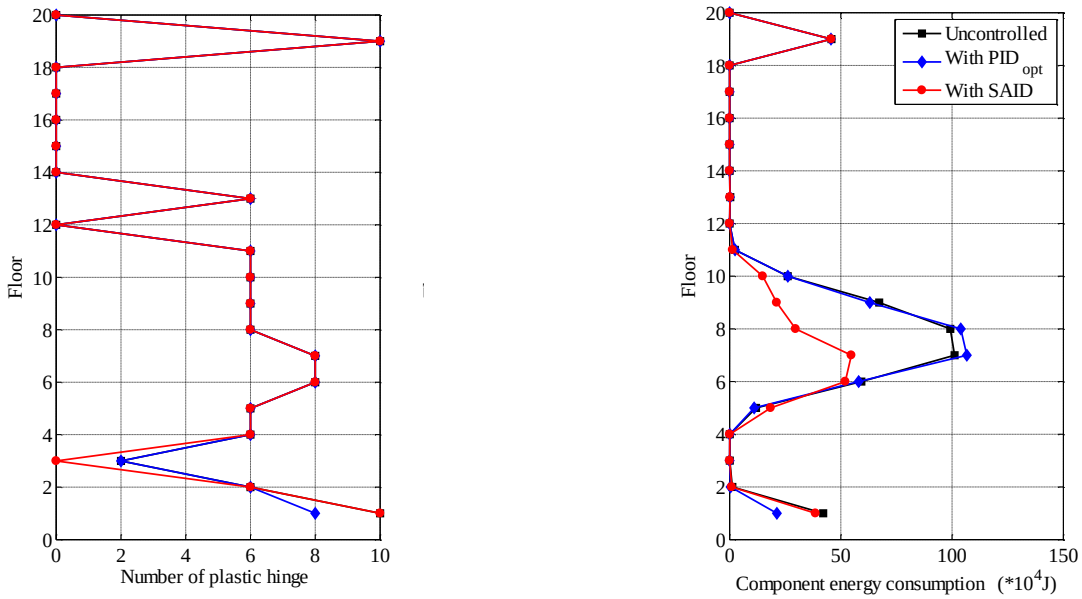

(a) number of plastic hinges (b) component energy consumption

Fig. 22 Comparison of nonlinear performance indexes under El Centro wave

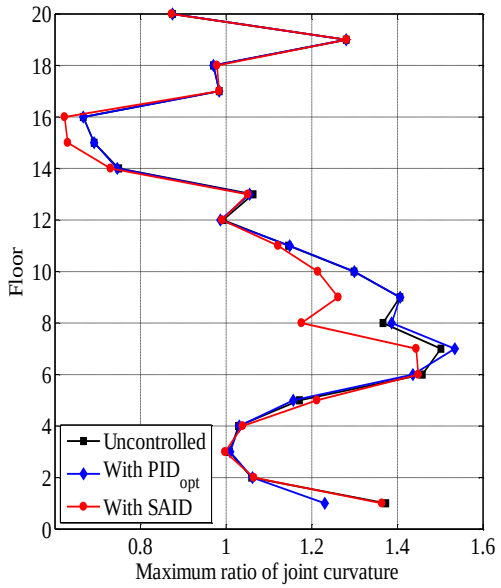

Fig. 23 Comparison of the maximum ratio of joint curvature and yield curvature at each floor under El Centro wave

5. Conclusions

A semi-active impact damper (SAID) compatible with a high-rise building is proposed in this paper. Details of the simulation method are introduced, and the parametric study is performed on both system parameters (mass ratio, damping ratio and rigid coefficient) and the intensity of excitation. The damping mechanism is also investigated, and some suggestions for a simple design procedure are proposed. In addition, an optimal particle impact damper (PID_{opt}) is also investigated as a control group, while the parameters of SAID remains the same to validate its superiority. The following conclusions pertaining to the vibration control mechanism of the proposed SAID on a realistic nonlinear high-rise building can be drawn:

- As the mass ratio increases, and as the rigid coefficient increases, and as the damping ratio decreases, the control effects of the SAID on the displacement response and structural nonlinear damage improve, and the improvement of the control effects is actually related to the increase of the nonlinear restoring force. In practical design, a proper smaller mass ratio is beneficial to the selection of other parameters.
- With suitable parameters, the SAID can significantly reduce the response of the main

structure, including not only the RMS displacement response but also the nonlinear behavior, compared with PID_{opt}. More energy flows to the SAID, and then the energy dissipated by the structure itself is reduced, hence protecting the main structure with a lower total components energy dissipation, and a smaller maximum ratio of joint curvature.

- The momentum exchange is the main damping mechanism of the SAID; as the momentum exchange increases, the control effect on the structural nonlinear damage improves. From this aspect, the mass ratio cannot be too small; considering the preceding conclusion, a mass ratio ranging from 0.005 to 0.01 is recommended. Moreover, the properly designed coefficient of restitution also has some beneficial effects on the efficiency of momentum exchange.

Acknowledgments

Financial supports from the National Natural Science Foundation of China (51478361), the Program of Shanghai Academic Research Leader (18XD1403900) and National Key Research and Development Program of China (2017YFC1500701) are highly appreciated. The work is also supported by the Fundamental Research Funds for the Central Government Supported Universities.

References

Afsharfard, A. and Farshidianfar, A. (2013), "Free vibration analysis of nonlinear resilient impact dampers", *Nonlinear Dynam.*, **73**(1-2),155-166.

Ahmad, N., Ranganath, R. and Ghosal, A. (2017), "Modeling and experimental study of a honeycomb beam filled with damping particles", *J.Sound Vib.*, **391**, 20-34. https://doi.org/10.1016/j.jsv.2016.11.011.

Bakre, S.V. and Jangid, R.S. (2004), "Optimum multiple tuned mass dampers for base excited damped main system", *Int. J. Struct. Stab. Dynam.*, **4**(4), 527-542. https://doi.org/10.1142/S0219455404001367.

Bakre, S.V. and Jangid, R.S. (2007), "Optimum parameters of tuned mass damper for damped main system", *Struct. Control Health Monit.*, **14**(3), 448-470. https://doi.org/10.1002/stc.166.

Bekdaş, G. and Nigdeli, S.M. (2013), "Mass ratio factor for optimum tuned mass damper strategies", *Int. J. Mech. Sci.*, **71**, 68-84. https://doi.org/10.1016/j.ijmecsci.2013.03.014.

Cheng, C.C. and Wang, J.Y. (2003), "Free vibration analysis of a resilient impact damper", *Int. J. Mech. Sci.*, **45**(4), 589-604. https://doi.org/10.1016/S0020-7403(03)00116-4.

Chung, L.L., Lai, Y.A., Yang, C.S.W., Lien, K.H. and Wu, L.Y. (2013), "Semi-active tuned mass dampers with phase control", *J. Sound Vib.*, **332**(15), 3610-3625. https://doi.org/10.1016/j.jsv.2013.02.008.

Dai, K.S., Wang, J.Z., Mao, R.F., Lu, Z. and Chen, S.E. (2017), "Experimental investigation on dynamic characterization and seismic control performance of a TLPD system", *Struct. Des. Tall Spec. Build.*, **26**(7), e1350. https://doi.org/10.1002/tal.1350.

Darabi, B. and Rongong, J.A, (2012) "Polymeric particle dampers under steady-state vertical vibrations", *J. Sound Vib.*, **331**(14), 3304-3316. https://doi.org/10.1016/j.jsv.2012.03.005.

De Angelis, M., Perno, S. and Reggio, A. (2012), "Dynamic response and optimal design of structures with large mass ratio TMD", *Earthq. Eng. Struct. D.*, **41**(1), 41-60. https://doi.org/10.1002/eqe.1117.

Egger, P. and Caracoglia, L. (2015), "Analytical and experimental investigation on a multiple-mass-element pendulum impact damper for vibration mitigation", *J. Sound Vib.*, **353**(1), 38-57. https://doi.org/10.1016/j.jsv.2015.05.003.

Fu, B., Jiang, H.J. and Wu, T. (2018), "Experimental study of seismic response reduction effects of particle damper using substructure shake table testing method", *Struct. Control Health Monit.*, **e2295**. DOI:10.1002/stc.2295.

Fujino, Y. and Abe, M. (1993), "Design formulas for tuned mass dampers based on a perturbation technique", *Earthq. Eng. Struct. D.*, **22**(10), 833-854. https://doi.org/10.1002/eqe.4290221002.

Han, B.K. and Li, C.X. (2008), "Characteristics of linearly distributed parameter-based multiple-tuned mass dampers", *Struct. Control Health Monit.*, **15**(6), 839-856. https://doi.org/10.1002/stc.222.

Housner, G.W., Bergman, L.A., Caughey, T.K., Chassiakos, A.G., Claus, R.O., Masri, S.F., Skelton, R.E., Soong, T.T., Spencer, B.F. and Yao, J.T.P. (1997), "Structural control: past, present, and future", *J. Eng.Mech. – ASCE*, **123**(9), 897-971. https://doi.org/10.1061/(ASCE)0733-9399(1997)123:9(897).

Jonathan, S. and Egidio, R. (2016), "Closed-form optimum tuning formulas for passive Tuned Mass Dampers under benchmark excitations", *Smart Struct. Syst.*, **17**(2), 231-256. http://dx.doi.org/10.12989/sss.2016.17.2.231.

Li, S. and Tang, J. (2017), "On vibration suppression and energy dissipation using tuned mass particle damper", *J. Vib. Acoust.*, **139**, 011008. doi: 10.1115/1.4034777.

Lin, C.C. and Lin, G.L. (2010), "Wang JF. Protection of seismic structures using semi-active friction TMD", *Earthq. Eng. Struct. D.*, **39**(6), 635-659. https://doi.org/10.1002/eqe.961.

Lu, X.L., Liu, Z.P. and Lu, Z. (2017a), "Optimization design and experimental verification of track nonlinear energy sink for vibration control under seismic excitation", *Struct. Control Health Monit.*, **24**(12), e2033. https://doi.org/10.1002/stc.2033.

Lu, X.L., Zhang, Q., Weng, D.G., Zhou, Z.G., Wang, S.S., Mahin, S.A, Ding, S.W. and Qian, F. (2017b), "Improving performance of a super tall building using a new eddy-current tuned mass damper", *Struct. Control Health Monit.*, **24**(3), e1882. https://doi.org/10.1002/stc.1882.

Lu, Z., Lu, X.L. and Masri, S.F. (2010), "Studies of the performance of particle dampers under dynamic loads", *J. Sound Vib.*, **329**(26), 5415-5433. https://doi.org/10.1016/j.jsv.2010.06.027.

Lu, Z., Masri, S.F. and Lu, X.L. (2011), "Parametric studies of the performance of particle dampers under harmonic excitation", *Struct. Control Health Monit.*, **18**(1), 79-98. https://doi.org/10.1002/stc.359.

Lu, Z., Chen, X.Y., Lu, X.L. and Yang, Z. (2016a), "Shaking table test and numerical simulation of an RC frame-core tube structure for earthquake-induced collapse", *Earthq. Eng. Struct. D.*, **45**(9), 1537-1556. https://doi.org/10.1002/eqe.2723.

Lu, Z., Wang, D.C., Masri, S.F. and Lu, X.L. (2016b), "An experimental study of vibration control of wind-excited high-rise buildings using particle tuned mass dampers", *Smart Struct. Syst.*, **18**(1), 93-115. http://dx.doi.org/10.12989/sss.2016.18.1.093.

Lu, Z., Chen, X.Y., Li, X.W. and Li, P.Z. (2017c), "Optimization and application of multiple tuned mass dampers in the vibration control of pedestrian bridges", *Struct. Eng. Mech.*, **62**(1), 55-64. https://doi.org/10.12989/sem.2017.62.1.055.

Lu, Z., Chen, X.Y., Zhang, D.C. and Dai K.S. (2017d), "Experimental and analytical study on the performance of

particle tuned mass dampers under seismic excitation", *Earthq. Eng. Struct. D.*, **46**(5), 697-714. https://doi.org/10.1002/eqe.2826.

Lu, Z., Chen, X.Y. and Zhou, Y (2017e), "An equivalent method for optimization of particle tuned mass damper based on experimental parametric study", *J. Sound Vib.*, **419**, 571-584. https://doi.org/10.1016/j.jsv.2017.05.048.

Lu, Z., Yang, Y.L., Lu, X.L. and Liu, C.Q. (2017f), "Preliminary study on the damping effect of a lateral damping buffer under a debris flow load", *Appl. Sciences-Basel*, **7**(2), 201. https://doi.org/10.3390/app7020201.

Lu, Z., Huang, B., Zhang, Q. and Lu, X.L. (2018a), "Experimental and analytical study on vibration control effects of eddy-current tuned mass dampers under seismic excitations", *J. Sound Vib.*, **421**, 153-165. https://doi.org/10.1016/j.jsv.2017.10.035.

Lu, Z., Huang, B. and Zhou, Y. (2018b), "Theoretical study and experimental validation on the energy dissipation mechanism of particle dampers", *Struct. Control Health Monit.*, **25**(4), e2125. https://doi.org/10.1002/stc.2125.

Lu, Z., Li, K., Ouyang, Y.T. and Shan, J.Z. (2018c), "Performance-based optimal design of tuned impact damper for seismically excited nonlinear structure", *Eng. Struct.*, **160**, 314-327. https://doi.org/10.1016/j.engstruct.2018.01.042.

Lu, Z., Wang, Z.X., Masri, S.F. and Lu, X.L. (2018d), "Particle Impact Dampers: Past, Present, and Future", *Struct. Control Health Monit.*, **25**, e2058. https://doi.org/10.1002/stc.2058.

Lu, Z., Wang, Z.X., Zhou, Y. and Lu, X.L. (2018e), "Nonlinear dissipative devices in structural vibration control: A review", *J. Sound Vib.*, **423**, 18-49. https://doi.org/10.1016/j.jsv.2018.02.052.

Masri, S.F., Miller, R.K., Dehghanyar, T.J. and Caughey, T.K. (1989), "Active parameter control of nonlinear vibrating structures", *J. Appl.Mech.*, **56**(3), 658-666. doi:10.1115/1.3176143.

Masri, S.F. and Chavakula, S. (1994), "Control of intelligent nonlinear adaptive systems under earthquake excitation", *J. Struct. Control*, **1**(1-2), 23-38. https://doi.org/10.1002/stc.4300010102.

Nagarajaiah, S. and Jung, H. (2014a), "Smart tuned mass dampers: recent developments", *Smart Struct. Syst.*, **13**(2), 173-176. http://dx.doi.org/10.12989/sss.2014.13.2.173.

Nagarajaiah, S. and Pasala D.T.R. (2014b), "Adaptive length SMA pendulum smart tuned mass damper performance in the presence of real time primary system stiffness change", *Smart Struct. Syst.*, **13**(2), 219-233. http://dx.doi.org/10.12989/sss.2014.13.2.219.

Nakamura, Y. and Watanabe, K. (2016), "Effects of balanced impact damper in structures subjected to walking and vertical seismic excitations", *Earthq. Eng. Struct. D.*, **45**(1), 113-128. https://doi.org/10.1002/eqe.2619.

Nayeri, R.D., Masri, S.F. and Caffrey, J.P. (2007), "Studies of the performance of multi-unit impact dampers under stochastic excitation", *J. Vib. Acoust.*, **129**(2), 239-251. doi:10.1115/1.2346694.

Ohtori, Y., Christenson, R.E., Spencer, B.F. and Dyke, S.J. (2004), "Benchmark control problems for seismically excited nonlinear building", *J. Eng. Mech.*, **130**(4), 366-385. https://doi.org/10.1061/(ASCE)0733-9399(2004)130:4(366).

Sanchez, M. and Manuel Carlevaro, C (2013), "Nonlinear dynamic analysis of an optimal particle damper", *J. Sound Vib.*, **332**(8), 2070-2080. https://doi.org/10.1016/j.jsv.2012.09.042.

Spencer Jr, B.F. and Nagarajaiah, S. (2003), "State of the art of structural control", *J. Struct. Eng.*, **129**(7), 845-856. https://doi.org/10.1061/(ASCE)0733-9445(2003)129:7(845).

Sun, C. and Nagarajaiah, S. (2014a), "Study on semi-active tuned mass damper with variable damping and stiffness under seismic excitations", *Struct. Control Health Monit.*, **21**(6), 890-906. https://doi.org/10.1002/stc.1620.

Sun, C., Nagarajaiah, S. and Dick, A.J. (2014b), "Family of smart tuned mass dampers with variable frequency under harmonic excitations and ground motions: closed-form evaluation", *Smart Struct. Syst.*, **13**(2), 319-341. http://dx.doi.org/10.12989/sss.2014.13.2.319.

Sun, C. (2018), "Semi-active Control of Offshore Wind Turbines under Multi-Hazards", *Mech. Syst. Signal Pr.*, **99**, 285-305. https://doi.org/10.1016/j.ymssp.2017.06.016.

Tributsch, A. and Adam, C. (2012), "Evaluation and analytical approximation of tuned mass damper performance in an earthquake environment", *Smart Struct. Syst.*, **10**(10), 1-25. http://dx.doi.org/10.12989/sss.2012.10.2.155.

Tsai, H.C. and Lin, G.C. (1993), "Optimum tuned-mass dampers for minimizing steady-state response of support-excited and damped systems", *Earthq. Eng. Struct. D.*, **22**(11), 957-973. https://doi.org/10.1002/eqe.4290221104.

Wang, Y., Liu, B., Tian, A. and Wei, D. (2016), "Experimental and numerical investigations on the performance of particle dampers attached to a primary structure undergoing free vibration in the horizontal and vertical directions", *J. Sound Vib.*, **371**, 35-55. https://doi.org/10.1016/j.jsv.2016.01.056.

Wang, Y., Liu, B., Tian, A., Wei, D. (2019), "Prediction methods for the damping effect of multi-unit particle dampers based on the cyclic iterations of a single-unit particle damper", *J. Sound Vib.*, **443**, 341-361. https://doi.org/10.1016/j.jsv.2018.10.035.

Wongprasert, N., Symans, M.D. (2004), "Application of a genetic algorithm for optimal damper distribution within the nonlinear seismic benchmark building", *J. Eng. Mech.*, **130**(4), 401-406. https://doi.org/10.1061/(ASCE)0733-9399(2004)130:4(401).

Xu, Z.D., Sha, L.F. and Zhang, X.C. (2013), "Design, performance test and analysis on magnetorheological damper for earthquake mitigation", *Struct. Control Health Monit.*, **20**(6), 956-970. https://doi.org/10.1002/stc.1509.

Xu, Z.D., Suo, S. and Lu, Y. (2016a), "Vibration control of platform structures with magnetorheological elastomer isolators based on an improved SAVS law", *Smart Materi. Struct.*, **25**, 065002.

Xu, Z.D., Xu F.H. and Chen, X. (2016b), "Intelligent Vibration Isolation and Mitigation of a Platform by Using MR and VE Devices", *J. Aerosp. Eng.*, **29**(4), 04016010. https://doi.org/10.1061/(ASCE)AS.1943-5525.0000604 .

Yao, B., Chen, Q., Xiang, H.Y. and Gao, X. (2014), "Experimental and theoretical investigation on dynamic properties of tuned particle damper", *Int. J. Mech. Sci.*, **80**, 122-130. https://doi.org/10.1016/j.ijmecsci.2014.01.009.

Zhang, K., Xi, Y.H., Chen, T.N. and Ma, Z.H. (2018), "Experimental studies of tuned particle damper: Design and characterization", *Mech. Syst. Signal Pr.*, **99**, 219-228. https://doi.org/10.1016/j.ymssp.2017.06.007.